Core-Sheath Fiber-Based Wearable Strain Sensor with High Stretchability and Sensitivity for Detecting Human Motions

Wenyue Li[1], Yanfen Zhou[1, 2], Yuhao Wang[1], Liang Jiang[*, 1, 2], Jianwei Ma[1, 2], Shaojuan Chen[*, 1, 2], Fenglei Zhou[1, 3]

W. Li, Y. Wang

College of Textiles and Clothing, Qingdao University, Qingdao 266071, China

wenyue.lee@outlook.com (W.L.); yuhao_wong@outlook.com (Y.W.)

Dr. Y. Zhou, Prof. L. Jiang, Prof. J. Ma, Prof. S. Chen

College of Textiles and Clothing, Qingdao University, Qingdao 266071, China

Eco-Textile Collaborative Innovation Center, Qingdao University, Qingdao, 266071, China

yanfen.zhou@qdu.edu.cn (Y.Z.); liang.jiang@qdu.edu.cn (L.J.); mjwfz@hotmail.com (J.M.); qdchshj@qdu.edu.cn (S.C.)

Dr. F. Zhou

College of Textiles and Clothing, Qingdao University, Qingdao 266071, China

Centre for Medical Image Computing, University College London, London, WC1V 6LJ, UK

fenglei.zhou@ucl.ac.uk (F.Z.)

Keywords: SBS, MWCNTs, core-sheath fibers, strain sensor, human motion monitoring

Abstract: Fiber-based strain sensor has been considered to be an important part of smart wearables due to its flexible performance, lightness and easily processing into various structures. However, low sensitivity of fiber-based strain sensors has limited their real-life applications for detecting human movements. In this work, a poly (styrene-butadiene-styrene) (SBS)/multi-walled carbon nanotubes (MWCNTs) core-sheath fiber (SSCCSF) strain sensor was fabricated via a simple and facile coaxial wet-spinning method. The cross-sectional morphology, the mechanical properties and the electromechanical performance of SSCCSFs were investigated.

The scanning electron microcopy results show that SSCCSFs have a bean-like shape in cross section with SBS as the core and SBS/MWCNTs as the sheath. Electromechanical performance evaluation confirms that the SSCCSF show a high sensitivity in a broad working range (Gauge Factor = 25832.77 at 41.5% strain) and excellent durability (5000 cycles at 10% strain). Furthermore, the SSCCSF displays outstanding sensing performance for detecting large motions in human movements including hand joint bending (such as knuckles and wrists) and subtle motions in physiological activities, involved in swallowing behavior, breathing and pulse beat. This study demonstrates the potential application of SSCCSFs for wearable electronics with activity monitoring sensor.

1. Introduction

Intelligent wearables have been penetrating into our everyday lives gradually due to their capacity of human health monitoring, human senses detection and movements assistance, etc. [1-4] For example, the track pants of Lumo Run have a variety of built-in sensors that can monitor the user's running rhythm, time in contact with the ground to help people find a better running sport form. Strain sensor, which can convert physical deformation into measurable electrical signals, is of great significance in smart technologies.[5, 6] However, conventional strain sensors consisting of metals or semiconductors cannot fulfil the demands of stretchable and comfortable wearing due to their toughness, poor stretchable performances and low sensitivity.[7, 8] Therefore, flexible strain sensors have gained considerable attention to solve these limitations and to develop more suitable structures that can fit the human body better.

Conductive polymer composites consisting of stretchable polymer and conductive fillers have been used extensively in fabricating flexible strain sensors.[5] Commonly used polymer

materials include thermoplastic polyurethane (TPU), polydimethylsiloxane (PDMS), Ecoflex and poly (styrene-butadiene-styrene) (SBS) while the conductive components mainly include carbon nanotubes (CNTs), graphene, carbon black (CB), metal nanoparticles and nanowires and intrinsically conductive polymers.[9-13]

Among various flexible strain sensors, fiber-based strain sensors, which have the advantages of tiny volume, high flexibility, changeable shape and weavability, have been used for a wide range of wearable electronic devices.[14, 15] For example, Li et al. fabricated a new fiber-shaped strain sensor made by electrospun TPU nanofiber yarns dipped with single-walled carbon nanotubes (SWCNTs) and multi-walled carbon nanotubes (MWCNTs), respectively. This high-performance strain sensor had broad working range of 100%, excellent stability during 2000 stretching-releasing cycles, but the gauge factor was low at about 1.67 in the strain range of 0–20% and 1.24 in the strain range of 20–100%. Furthermore, different human motions such as neck bending, wrist bending, knee joint bending, elbow bending and finger joint bending could be monitored accurately and constantly by using the strain sensors.[16] Wang et al. utilized the wet-spun method to compound TPU and MWCNTs together to prepare fibers as the strain sensor, which displayed an ultra-wide workable strain range of 320%, a relatively high gauge factor of 22.2 within 160% strain and 97.1 for 160–320% strain and awesome durability for 9700 stretching-releasing cycles at a constant strain 100%.[17] Bautista-Quijano et al. prepared a flexible SBS/conductive thermoplastic urethane (C-TPU) blend filament by using melt extruding process. The SBS/C-TPU hybrid filament exhibited wide workable detection range (of 50% strain), good elongation at break (above 150%) and a relatively high sensitivity (gauge factor of 26), expecting good potentiality for applications.[18] Nevertheless, although most

previously reported fiber-shaped strain sensors had a wide workable range of more than 100%, even as high as 300%, but the low sensitivity of these sensors has significantly limited their real-life applications for the detection of subtle human movements such as pulse or breathing signals. Microstructural design including multilayer structures and hollow-monolith structures is considered as an effective method to obtain high-performance strain sensor.[19, 20] Among them, the core-sheath structure with various performances in different layers have attracted widespread attention for fabricating flexible sensors in recent years.[21, 22]

In this work, a highly sensitive and stretchable core-sheath fiber-based strain sensor based on SBS and MWCNTs was fabricated through a simple and facile coaxial wet-spinning method. The morphology of the core-sheath structure and the mechanical performance were investigated. The stretchability and electromechanical stability were evaluated by recording the change of electrical conductivity when the fibers were subjected to one-shot stretching and repeated stretching-releasing deformations. Finally, the sensing performance of the core-sheath fiber was demonstrated by detecting various human large motions (such as knuckles and wrists) and subtle motions in physiological activities, involved in swallowing behavior, breathing, pulse beat.

2. Experimental Section

2.1. Materials

Multi-walled carbon nanotubes (MWCNTs, >97%, pipe diameter = 3-15 nm, tube length = 15-30 μm) was carboxylated and bought from Turing Evolution Technology Co., Ltd. (Shenzhen, China). Poly (styrene-butadiene-styrene) (SBS) with a butadiene/styrene weight ratio of 60/40 was bought from Sinopec Group Maoming Petrochemical Co., Ltd., China. Both

tetrahydrofuran (THF, 99.5%, analytical reagent) as solvents and ethanol absolute (≥99.7%, analytical reagent) as coagulation bath were provided by Sinopharm Chemical Reagent Co., Ltd. (Shanghai, China).

2.2. Fabrication of core-sheath fibers

Figure 1 illustrates the fabrication process of core-sheath fibers through the wet spinning method. Firstly, the SBS solution to fabricate the core layer was prepared by dissolving SBS pellets (5.92 g) in 20 ml THF and magnetically stirred for 18 h at room temperature until completely dissolved. Secondly, the SBS/MWCNTs suspension to fabricate the conductive sheath layer was prepared as follows: MWCNTs were dispersed in 20 ml THF under ultrasonication for 2 h to form the suspension with different MWCNTs concentration; Then, SBS pellets were added into the above MWCNTs suspension and magnetic stirred for 18 h; The mixture was treated under ultrasonication for 1 h finally to form a spinning solution. At last, pure SBS as the inner layer and SBS/MWCNTS mixture as the outer layer were injected into the ethanol coagulation bath with a coaxial needle (18 G/25 G) at an extrusion speed of 2 ml·h^{-1}. The obtained fibers were dried in vacuum oven at 60 °C for 2 h. Before the preparing procedures, SBS pellets were dried in a vacuum oven at 60 °C for 24 h to remove the absorbed moisture. The obtained SBS-SBS/MWCNTs core-sheath fiber (SSCCSF) was denoted as SSCCSF-x, in which x represents the weight percentage of the MWCNTs in the sheath layer. For instance, SSCCSF-7 means that the weight percentage of MWCNTs in the SBS/MWCNTs sheath layer was 7 %. Similarly, SSCCSF-9, SSCCSF-11, SSCCSF-13 represents the SBS-SBS/MWCNTs core-sheath fiber with an SBS/MWCNTs sheath layer containing 9%, 11% and 13% (weight percentage) MWCNTs, respectively.

2.3. Characterization

The surface morphology of the fibers was observed by using a scanning electron microscope (SEM, TESCAN VEGA3, Czech) with various magnifications at an accelerated voltage of 10 kV. The cryo-fractured samples were coated with a thin layer of gold before observation.

The mechanical property tests including tensile breaking tests and elastic recovery rate tests were conducted on a universal tensile testing machine (Instron 5965, United States). For tensile breaking tests, ten tests were conducted for each sample with the fiber grip length of 20 mm and the stretching rate of 200 mm·min^{-1}, the average value of tensile strength and elongation at break was used. For elastic recovery rate tests, three tests were conducted for each sample and the fiber grip length was 20 mm with a stretching-recovering rate of 20 mm·min^{-1}. The average elastic recovery rate was used.

The interface interaction of SSCCSFs were investigated by using a fourier transform infrared spectroscopy (FTIR, Nicolet iS10, United States) at room temperature. The spectrum was collected in the wavenumber ranging 4000-500 cm^{-1} at scanning times of 32 and resolution of 4 cm^{-1}.

Thermo gravimetric analysis was carried out by utilizing a DSC/TG synchronous thermal analyzer (STA449 F3 Jupiter, Bavaria, Germany). The measurements were conducted under a nitrogen atmosphere and the samples were heated from 40 °C to 800 °C at a rate of 20 °C·min^{-1}.

The electromechanical properties were evaluated by a two-probe method with copper clamps employing a digital multimeter (KEYSIGHT B2901A, United States) which was equipped with a stepper motor to induce various tensile deformations of samples and the data was recorded

on-line through a computer connected to the instrument. In the study of human motions monitoring, SSCCSF with a length of 2 cm was chosen to fix on rubber membrane with a size of 2 cm × 5 cm in order to ensure insulation from human body detection. Both ends of the fiber sample were dipped into colloidal silver ink and connected with copper tapes. Then, the SSCCSF sensor was mounted onto human body through band aid. Before conducting the experimental study on one human volunteer, the participant read and signed a consent form.

3. Results and discussion

3.1. Morphology, thermal behaviour and interface interaction

The SEM images of pure SBS fibers, SBS/MWCNTs composite fibers and SBS-SBS/MWCNTs core-sheath fibers are shown in **Figure 2**. It can be seen that pure SBS fiber (Figure 2a) and the SBS/MWCNTs composite fiber (Figure 2b) all have a "bean" shape cross-section attributed to the fiber shrinking during the solidification process.[23] As previously reported, during the wet-spinning process, there was a difference in the mass transfer rate which was manifested in irregular cross-sections of the fabricated fibers when the extraction rate of the solvent used in the spinning solution into the coagulation bath was lower than the diffusion rate of the coagulating bath into the fiber.[24, 25] In addition, pure SBS fibers have a uniform and compact internal structure (Figure 2a'), whereas in contrast, for the SBS/MWCNTs composite fiber, obvious nano-aggregates was observed (Figure 2b', red dotted frame) due to the addition of MWCNTs. The core-sheath fiber SSCCSF-11 (Figure 2c) had a "bean" structure cross-section as well and the core-sheath structure (Figure 2c') can be clearly seen, with the thickness of sheath layer being 62.14 ± 9.0 μm, when compared to the pure SBS fiber and SBS/MWCNTs composite fiber. From Figure 2c'' and 2c''', it can be seen that the core layer of SSCCSF-11

shows a uniform structure as that of pure SBS while the sheath layer shows obvious nano-aggregates embedded in the SBS matrix.

TGA (**Figure S1. Supporting Information**) was utilized to determine the practical content of MWCNTs in the core-sheath fiber. It turned out that the mass content of MWCNTs in the SSCCSF-7, SSCCSF-9, SSCCSF-11 and SSCCSF-13 core-sheath fiber is 0.77%, 1.59%, 2.63% and 3.62%, respectively. The FTIR spectra of SSCCSFs and pure SBS fibers were used to analyze the interface interaction between the MWCNTs and SBS. As displayed in Figure S2, the characteristic bands of styrene and butadiene can be observed in the spectrum of pure SBS.[26-29] The spectrum of the core-sheath fiber also show the characteristic bands of SBS, but no new peaks and band energy deviation are identified, suggesting no chemical interactions between the SBS macromolecular chain and the MWCNTs.[27]

3.2. Mechanical property

Figure 3a shows the typical stress-strain curves of SSCCSFs with different content of MWCNTs and Figure 3b shows the average values of tensile strength and elongation at break. It can be seen that as the content of MWCNTs increases, the tensile strength decreases from 19.86 ± 1.92 MPa to 14.79 ± 1.23 MPa and the elongation at break decreases from 1438.02 ± 140.54 % to 1181.85 ± 96.25 %. This is because high content of MWCNT caused serious agglomeration due to the strong Van der Waals force and limited the movement of SBS molecular chains.[19] Although SSCCSF-13 has the lowest tensile strength and elongation at break, it is still within a reasonable level for stretchable strain sensors.[32, 33]

Figure 4 displays the elastic recovery performance of the core-sheath fibers at a rate of 20 mm·min^{-1}. The elastic recovery rate was determined by using equation (1):

$$e_\varepsilon = \frac{\varepsilon - \varepsilon_R}{\varepsilon} \times 100\% \qquad (1)$$

Where ε represents the tensile strain, ε_R is the residual strain after tensile-recovery tests.[25, 34]

It can be observed from Figure 4a that the loading and unloading paths of the stress-strain curves are different for each core-sheath fiber with different MWCNTs contents and the corresponding elastic recovery rate of SSCCSF-7, SSCCSF-9, SSCCSF-11 and SSCCSF-13 is 84.49%, 86.11%, 85.03% and 84.01% respectively, suggesting mechanical hysteresis during tensile testing. This is attributed to the slippage occurring between MWCNTs, MWCNTs and SBS molecular chains, and SBS molecular chains during stretching.[34] Figure 4b shows the elastic recovery test of SSCCSF-11 with different strains of 50%, 100%, 200%, 500% and 800%. It can be seen that as the applied strain increases, it becomes more difficult for the fibers to recover to the original state. Continuous cyclic test results for up to 7 cycles of SSCCSF-11 under 50% strain are shown in Figure 4c-d. It can be seen that the tensile and recovery curve in the first loading and unloading cycle follows different trend from other six cycles under the same tensile strain. During the first 6 continuous cycles, each curve tends to move farther away from the original position than the previous cycle. However, compared to the previous cycle, the increasing amplitude of hysteresis was reduced. Furthermore, when the 7th tensile test is employed 30s after the 6th cycle, the path of its stress-strain curve becomes closer to the curve trend of the 1st cycle in comparison with that of the 6th cycle (Figure 4d), indicating that the elastic recovery performance of SSCCSF could be time-dependent.[35]

3.3. Electrical properties

The conductivity was utilized to characterize the electrical properties of SSCCSFs. As is illustrated in the **Figure 5**, SSCCSFs have an increasing conductivity with the MWCNTs content increasing and the relationship can be described well by using equation (2) depending

on the statistical percolation theory.[22,30]

$$\sigma=\sigma_0(m-m_c)^t \tag{2}$$

where σ is the conductivity of composites at a given filler content, σ_0 is a scaling factor, m is the filler mass content, m_c is the percolation threshold, and t is critical resistance exponent, which is dependent on the geometry of the MWCNTs conductive networks.

The experimental data were well fitted (R^2=0.91229) in line with the equation (2), giving a t of 1.54 and m_0 of 6.39%. Generally speaking, the t of a two-dimensional system is approximately 1.1−1.3, and the t of a three-dimensional system is between 1.6 and 2.0, which means that a nearly three-dimensional conductive network has been achieved in SSCCSFs. [31]

3.4. Electromechanical properties

The strain value (ε) is defined as the ratio of the length change ($\varDelta\varepsilon$) to the initial length (ε_0) of the core-sheath fiber. The relative resistance change ($\varDelta R/R_0$) is defined as the ratio of the resistance change ($\varDelta R$) to the original resistance (R_0). Gauge Factor (GF) is defined as the ratio of $\varDelta R/R_0$ to ε, applying to evaluate the strain sensitivity. Here the strain value (ε), the relative resistance change ($\varDelta R/R_0$) and the gauge factor (GF) were used to evaluate the electromechanical properties of the SSCCSF based strain sensors.

Figure 6 illustrates the real-time change of electrical resistance with tensile strain for the SSCCSFs with various MWCNTs contents. The tensile speed was controlled at 5 mm·min^{-1}. As shown in Figure 6a, the value of $\varDelta R/R_0$ increases rapidly with the increasing strain for SSCCSF with each MWCNTs content, indicating an excellent sensitivity as a strain sensor. It can also be seen from Figure 6a that the changes in $\varDelta R/R_0$ of SSCCSF with increasing strain vary with the MWCNTs content. For example, SSCCSF-7 shows a low workable range of 14.83% with GF

of 9021.03, whereas in contrast, SSCCSF-11 has the highest sensitivity of 25832.77 (at 41.5%

strain) and SSCCSF-13 has the largest working range of 44.0% with GF of 12768.32. This

suggests that the content of MWCNTs has a great influence on the electromechanical

performance as strain sensors. The stretching-releasing test for SSCCSFs with different

MWCNTs contents was also conducted to reveal the response of the fibers to different strains.

It can be seen from Figure 6b that the SSCCSF-based sensors could respond to strain as low as

0.5% and 1% while showing a relative stable response to various strain ranges. However, the

fibers could not return to the original resistance after stretching, especially at the beginning

several cycles, indicating the hysteresis behavior as well due to the time-dependent mechanical

response.[4, 35-37]

The strain sensing behaviors of the core-sheath fibers under various strain ranges, tensile rates

and repeated stretching-releasing cycles were further studied. SSCCSF-11 was used as an

example because of its extraordinary sensing properties including a large working range,

relatively high structural stability and high sensitivity. **Figure 7a** shows the curve fitting to the

experimental data acquired from the testing of electrical response of SSCCSF-11 to applied

strain, which can be theoretically analyzed based on the tunnel effect.[34, 38] According to the

model reported previously,[17, 25, 39] the total electrical resistance R of SSCCSFs can be defined

with equations (3) and (4):

$$R = \left(\frac{L}{N} \right) \left(\frac{8\pi hs}{3\gamma a^2 e^2} \right) \exp(\gamma s) \tag{3}$$

$$\gamma = \frac{4\pi \sqrt{2m\varphi}}{h} \tag{4}$$

Where N represents the number of conducting paths, L represents the particles forming a single

conducting path, s is the smallest distance between adjacent MWCNTs, h is the Plank constant, a^2 is the effective cross-section and e is the electron change, respectively. Furthermore, m represents the electron mass and φ represents the height of potential barrier between adjacent MWCNTs.

When an external force is applied on SSCCSFs, the resistance would increase due to the destruction of conductive MWCNT networks. Assuming that the separation between MWCNTs varies from s_0 (initial particle separation) to s under the applied force and the number of conductive network decreased from N_0 (the number of conductive pathways in initial state) to N, s and N can be expressed as equations (5) and (6), respectively:

$$s = s_0\left(1 + C\varepsilon\right) \tag{5}$$

$$N = \frac{N_0}{\exp\left(M\varepsilon + W\varepsilon^2 + U\varepsilon^3 + V\varepsilon^4\right)} \tag{6}$$

Where C, M, W, U and V are constants. Substituting equations (5) and (6) into equation (3) yields:

$$\begin{aligned}
\frac{\Delta R}{R_0} = \frac{R - R_0}{R_0} &= \left(\frac{sN_0}{Ns_0}\right)\exp\left[\gamma\left(s - s_0\right)\right] - 1 \\
&= \left(1 + C\varepsilon\right)\exp\left[\left(M + \gamma bs_0\right)\varepsilon + W\varepsilon^2 + U\varepsilon^3 + V\varepsilon^4\right] - 1
\end{aligned} \tag{7}$$

It can be seen from Figure 7a that the experimental result is in good agreement with the theoretical value with R^2 value of 0.99825.

Figure 7b and c shows the change of $\Delta R/R_0$ in 30 stretching-releasing cycles with different applied strains at a fixed rate of 10 mm·min^{-1} and with different tensile rates at a constant strain of 10% strain for the SSCCSF-11, respectively. From Figure 7b it can be seen that the maximum $\Delta R/R_0$ of the SSCCSF-11 increases as the strain increases. Moreover, the peaks of $\Delta R/R_0$

gradually decreases in the first ten cycles approximately and then seems to stabilize. This is attributed to the formation of stable conductive pathways via the constant destruction and reconstruction of the MWCNTs networks during the stretching-releasing process.[40, 41] Figure 7c revels that a slow speed from 1 mm·min^{-1} to 10 mm·min^{-1}, has a weak effect on $\Delta R/R_0$, whereas in contrast, the maximum $\Delta R/R_0$ significantly changes as the speed increases to 50 mm·min^{-1} and 100 mm·min^{-1}, resulting in a diminished sensing stability. To evaluate the durability and reproducibility of the sensing ability of SSCCSF-11 sensor, 5000 cycles of stretching-releasing test was conducted at a constant strain range of 0-10% strain, the change in $\Delta R/R_0$ with the cycles is shown in Figure 7d. It can be seen that the resistance decreases at the beginning shown in region I and then tended to be stable after experiencing several stretching-releasing cycles shown in region II-VI, indicating an outstanding stability as discussed before.

The mechanism of electrical resistance change during the stretching-releasing process of SSCCSF-11 is illustrated in **Figure 8**. When an external force is applied to induce a deformation on the fibers (Figure 8a-b), the overlapping area of the MWCNTs decline and the distance between MWCNTs increases, resulting in the destruction of the conductive pathway (Figure 8a-b, red dotted frame). When the deformation is less than 20%, a few pathways is broken and a gentle increment appears in the electrical resistance; When the deformation is higher than 20%, more conductive pathways experience irreversible destruction, which result in the rapid and sharp change of $\Delta R/R_0$ as shown in Figure 7a. Simultaneously, a few new conductive pathways are probably formed (Figure 8a-b, white dotted frame). The stretching process lead to an increase in electrical resistance macroscopically. When the strain sensor is subjected to

releasing (Figure 8b-c), the electrical resistance decreases with the reconstruction of the MWCNTs conductive networks (Figure 8b-c, red dotted frame). Due to the stretching process experienced irreversible destruction, the strain sensor could not return completely to the original resistance (Figure 8b-c, yellow dotted frame). After several stretching and releasing processes, the destruction and reconstruction of the conductive network reached equilibrium, leading to a stable change in the relative electrical resistance.[17, 25, 42]

3.5. Application of SSCCSF sensors in Human Motion Monitoring

Finally, the applications of SSCCSF in monitoring human motions including the joint bending (the interphalangeal joint and the wrist joint), and subtle motions in physiological activities, involved in swallowing behavior, breathing, pulse beat were demonstrated. **Figure 9a** and b displays the real-time monitoring of human finger motion and the condition of the interphalangeal joint bending with different angles of 30 °, 60 ° and 90 °, respectively. It can been observed that the value of $\Delta R/R_0$ increases along with the bending of the interphalangeal joint and decreases with the joint straightening. Furthermore, the maximum value of $\Delta R/R_0$ increases as the angle increases, indicating of the ability to distinguish different degrees of bending deformation. Figure 9c and d exhibit the wrist joint motion and the condition of the wrist bending with different angles of 30 °, 45 ° and 60 °, respectively. It can be seen that the $\Delta R/R_0$ increases during the bending process and then decreases during the unbending process, indicating that SSCCSF is highly sensitive to the angle change. The effects of minor strain changes during swallowing, deep and normal breathing, and pulse beating before and after exercise on $\Delta R/R_0$ were recorded. As shown in Figure 9e-f, the SSCCSF sensor is capable of detecting the subtle human motions, although the changes in the electrical conductivity is

relatively less stable than those caused by the large-scale motions.

4. Conclusions

In this study, highly stretchable and sensitive SBS-SBS/MWCNTs core-sheath fibers (SSCCSF) have been fabricated via a simple and facile coaxial wet-spinning method. The resultant core-sheath fiber exhibits a bean-like cross-section due to the mass transfer rate, with SBS as the core and SBS/MWCNTs as the sheath. The electromechanical testing of SSCCSFs with various MWCNTs contents show that the SBS-SBS/11% MWCNTs core-sheath fibers (SSCCSF-11) has excellent sensing properties including high sensitivity, a relative broad working range (GF=25832.77 at 41.5% strain) and high durability (5000 cycles at 10% strain). Furthermore, human motion monitoring experiments demonstrates that the prepared SSCCSF sensor displays excellent sensing performance in detecting muscle including hand joint bending (such as knuckles and wrists), and subtle motions such as swallowing, breathing and pulse beat. This study provides a simple method to fabricate a high performance fiber-based strain sensor for directly and precisely monitoring the subtle and large human motions, showing the potential applications on wearable electronics with activity monitoring sensor.

Conflict of Interest

The authors declare no conflict of interest.

Reference

[1] I. Awolusi, E. Marks, M. Hallowell, *Automat. Constr.* **2018**, *85*, 96.

[2] J. Di, X. Zhang, Z. Yong, Y. Zhang, D. Li, R. Li, Q. Li, *Adv. Mater.* **2016**, *28*, 10529.

[3] W. Li, Y. Zhou, Y. Wang, Y. Li, L. Jiang, J. Ma, S. Chen, *Macromol. Mater. Eng.* **2020**, *305*, 1900736.

[4] M. Amjadi, K.-U. Kyung, I. Park, M. Sitti, *Adv. Funct. Mater.* **2016**, *26*, 1678.

[5] S. Seyedin, P. Zhang, M. Naebe, S. Qin, J. Chen, X. Wang, J. M. Razal, *Mater. Horiz.* **2019**, *6*, 219.

[6] Y. Wang, W. Li, Y. Zhou, L. Jiang, J. Ma, S. Chen, S. Jerrams, F. Zhou, *J. Mater. Sci.* **2020**, *55*, 12592.

[7] T. Yan, Z. Wang, Z.-J. Pan, Curr. Opin. *Solid State Mater. Sci.* **2018**, *22*, 213.

[8] S. Yu, X. Wang, H. Xiang, L. Zhu, M. Tebyetekerwa, M. Zhu, *Carbon*, **2018**, *140*, 1.

[9] C. Yan, J. Wang, W. Kang, M. Cui, X. Wang, C. Y. Foo, K. J. Chee, P. S. Lee, *Adv. Mater.* **2014**, *26*, 2022.

[10]V. B. Nam, D. Lee, *Nanomaterials*, **2016**, *6*, 47.

[11]H. Qi, B. Schulz, T. Vad, J. Liu, E. Mader, G. Seide, T. Gries, *ACS Appl. Mater. Interfaces* **2015**, *7*, 22404.

[12]S.-T. Hsiao, C.-C. M. Ma, H.-W. Tien, W.-H. Liao, Y.-S. Wang, S.-M. Li, Y.-C. Huang, *Carbon*, **2013**, *60*, 57.

[13] Y. Zhou, Z. Sun, L. Jiang, S. Chen, J. Ma, F. Zhou. *Appl. Surf. Sci.* **2020**, *533*, 147431.

[14]W. Zeng, L. Shu, Q. Li, S. Chen, F. Wang, X. M. Tao, *Adv. Mater.* **2014**, *26*, 5310.

[15] P. Xue, X. Tao, M.-Y. Leung, H. Zhang, *Wearable electronics and photonics*, CRC Press, Boca Raton, FL **2005**, p. 81.

[16] Y. Li, B. Zhou, G. Zheng, X. Liu, T. Li, C. Yan, C. Cheng, K. Dai, C. Liu, C. Shen, Z. Guo, *J. Mater. Chem. C* **2018**, *6*, 2258.

[17] X. Wang, H. Sun, X. Yue, Y. Yu, G. Zheng, K. Dai, C. Liu, C. Shen, *Compos. Sci. Technol.* **2018**, *168*, 126.

[18] J. R. Bautista-Quijano, R. Torres, O. Kanoun, in *NANOfIM 2018: International Conference on Nanotechnology for Instrumentation and Measurement* (IEEE2018), 1.

[19] J. Gao, X. Wang, W. Zhai, H. Liu, G. Zheng, K. Dai, L. Mi, C. Liu, C. Shen, *ACS Appl. Mater. Interfaces* **2018**, *10*, 34592.

[20] Z. Wang, J. Ren, R. Liu, X. Sun, D. Huang, W. Xu, J. Jiang, K. Ma, Y. Liu, *Composites, Part A* **2020**, *136*, 105957.

[21] Y. Zhang, W. Zhang, G. Ye, Q. Tan, Y. Zhao, J. Qiu, S. Qi, X. Du, T. Chen, N. Liu, *Adv. Mater. Technol.* **2019**, *5*, 1900880.

[22] Z. Tang, S. Jia, F. Wang, C. Bian, Y. Chen, Y. Wang, B. Li, *ACS Appl. Mater. Interfaces* **2018**, *10*, 6624.

[23] G.-q. Peng, X.-h. Zhang, Y.-f. Wen, Y.-g. Yang, L. Liu, *J. Macromol. Sci., Part B: Phys.* **2008**, *47*, 1130.

[24] M. Z. Seyedin, J. M. Razal, P. C. Innis, G. G. Wallace, *Adv. Funct. Mater.* **2014**, *24*, 2957.

[25] X. Wang, S. Meng, M. Tebyetekerwa, Y. Li, J. Pionteck, B. Sun, Z. Qin, M. Zhu, *Composites, Part A* **2018**, *105*, 291.

[26] P. Costa, S. Ribeiro, G. Botelho, A. V. Machado, S. Lanceros Mendez, *Polym. Test.*

2015, *42*, 225.

[27] P. Costa, C. Silvia, J. C. Viana, S. Lanceros Mendez, *Composites, Part B* **2014**, *57*, 242.

[28] P. Costa, J. Silva, A. Ansón-Casaos, M. T. Martinez, M. J. Abad, J. Viana, S. Lanceros-Mendez, *Composites, Part B* **2014**, *61*, 136.

[29] L. B. Canto, G. L. Mantovani, E. R. deAzevedo, T. J. Bonagamba, E. Hage, L. A. Pessan, *Polym. Bull.* **2006**, *57*, 513.

[30] H. Liu, Y. Li, K. Dai, G. Zheng, C. Liu, C. Shen, X. Yan, J. Guo, Z. Guo, *J. Mater. Chem. A,* **2016**, *4, 1.*

[31] H. Zhao, J. Bai, *ACS Appl. Mater. Interfaces*, **2015**, *7, 18.*

[32] P. Costa, M. F. Carvalho, V. Correia, J. C. Viana, S. Lanceros-Mendez, *ACS Appl. Nano Mater.* **2018**, *1*, 3015.

[33] S. Lee, S. Shin, S. Lee, J. Seo, J. Lee, S. Son, H. J. Cho, H. Algadi, S. Al-Sayari, D. E. Kim, T. Lee, *Adv. Funct. Mater.*, **2015**, *25*, 3114.

[34] S. Yu, X. Wang, H. Xiang, M. Tebyetekerwa, M. Zhu, *Sci. China Mater.* **2019,** *62*, 995.

[35] R. Zhang, H. Deng, R. Valenca, J. Jin, Q. Fu, E. Bilotti, T. Peijs, *Compos. Sci. Technol.*, **2013**, *74*, 1.

[36] H. Liu, Q. Li, S. Zhang, R. Yin, X. Liu, Y. He, K. Dai, C. Shan, J. Guo, C. Liu, C. Shen, X. Wang, N. Wang, Z. Wang, R. Wei, Z. Guo, *J. Mater. Chem. C*, **2018**, *6*, 12121.

[37] Y. Lu, M. C. Biswas, Z. Guo, J.-W. Jeon, E. K. Wujcik, *Biosens. Bioelectron.* **2019**, *123*, 167.

[38] C. Lee, L. Jug, E. J. A. P. L. Meng, *Appl. Phys. Lett.* **2013**, *102*, 183511.

[39] M. Ji, H. Deng, D. Yan, X. Li, L. Duan, Q. Fu, *Compos. Sci. Technol.* **2014**, *92*, 16.

[40] L. Duan, S. Fu, H. Deng, Q. Zhang, K. Wang, F. Chen, Q. Fu, *J. Mater. Chem. A* **2014**, *2*, 17085.

[41] H. Liu, J. Gao, W. Huang, K. Dai, G. Zheng, C. Liu, C. Shen, X. Yan, J. Guo, Z. Guo, *Nanoscale* **2016**, *8*, 12977.

[42] J. Huang, D. Li, M. Zhao, A. Mensah, P. Lv, X. Tian, F. Huang, H. Ke, Q. Wei, *Adv. Electron. Mater.* **2019**, *5*, 1900241.
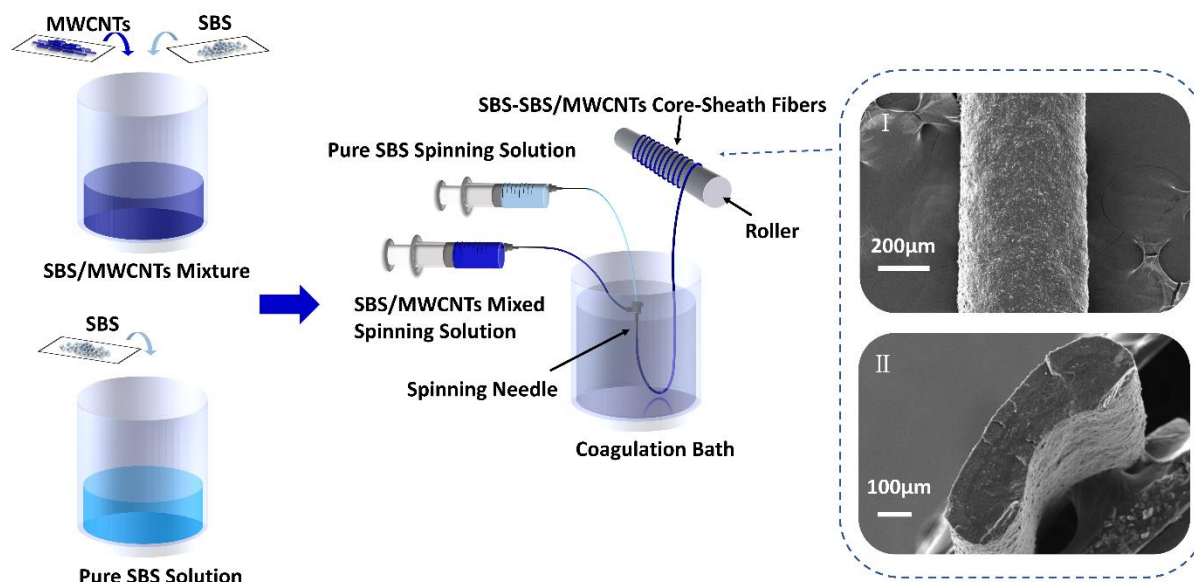
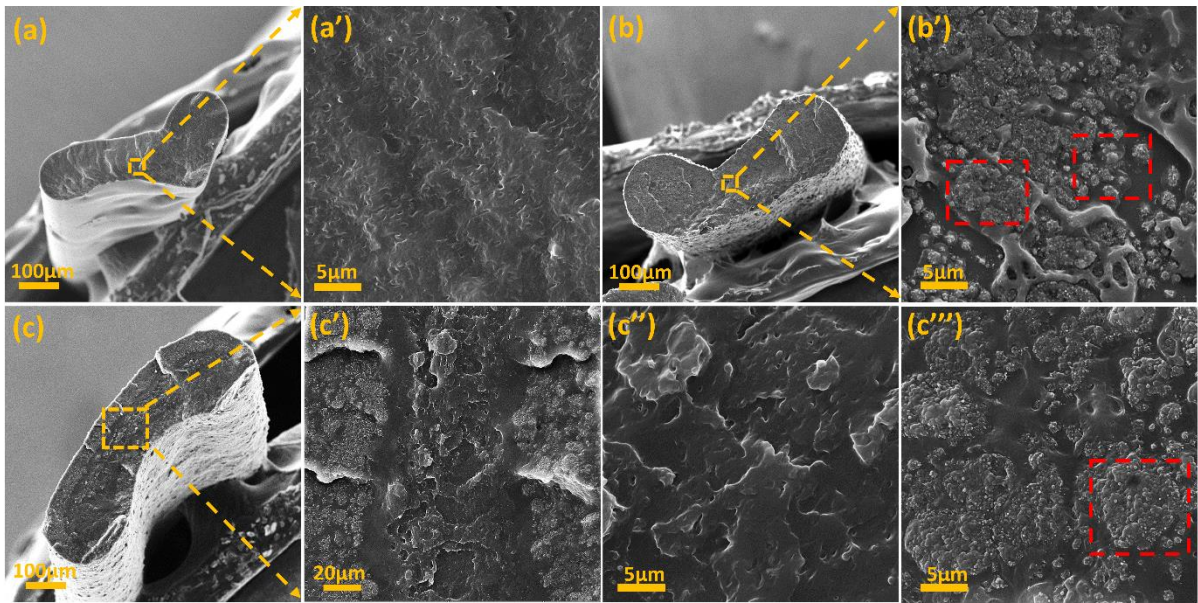**Figure 1. A schematic illustration of the procedure for preparing SBS-SBS/MWCNTs core-sheath fiber.**

Figure 2. SEM photographs of the cross section of pure SBS fiber (a-a'), SBS/MWCNTs composite fiber (b-b') and SBS-SBS/MWCNTs core-sheath fiber (SSCCSF) (c-c''') (c'' is the SBS inner layer and c''' is the outer SBS/MWCNTs layer). The MWCNTs concentration is 11%.
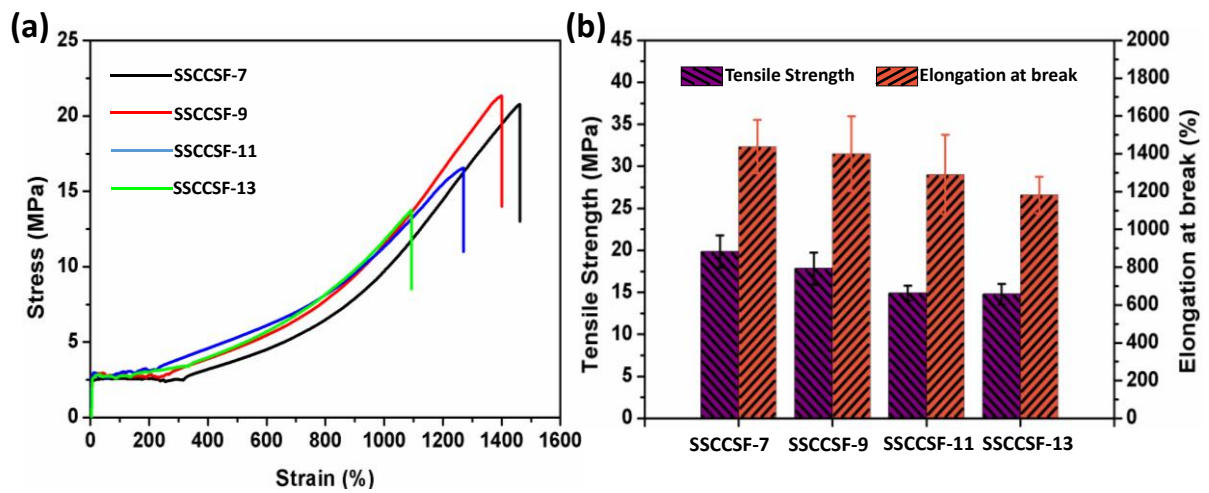
Figure 3. (a) Stress-strain curves and (b) Bar graph of the tensile strength and elongation at break of SSCCSFs with different MWCNTs content.
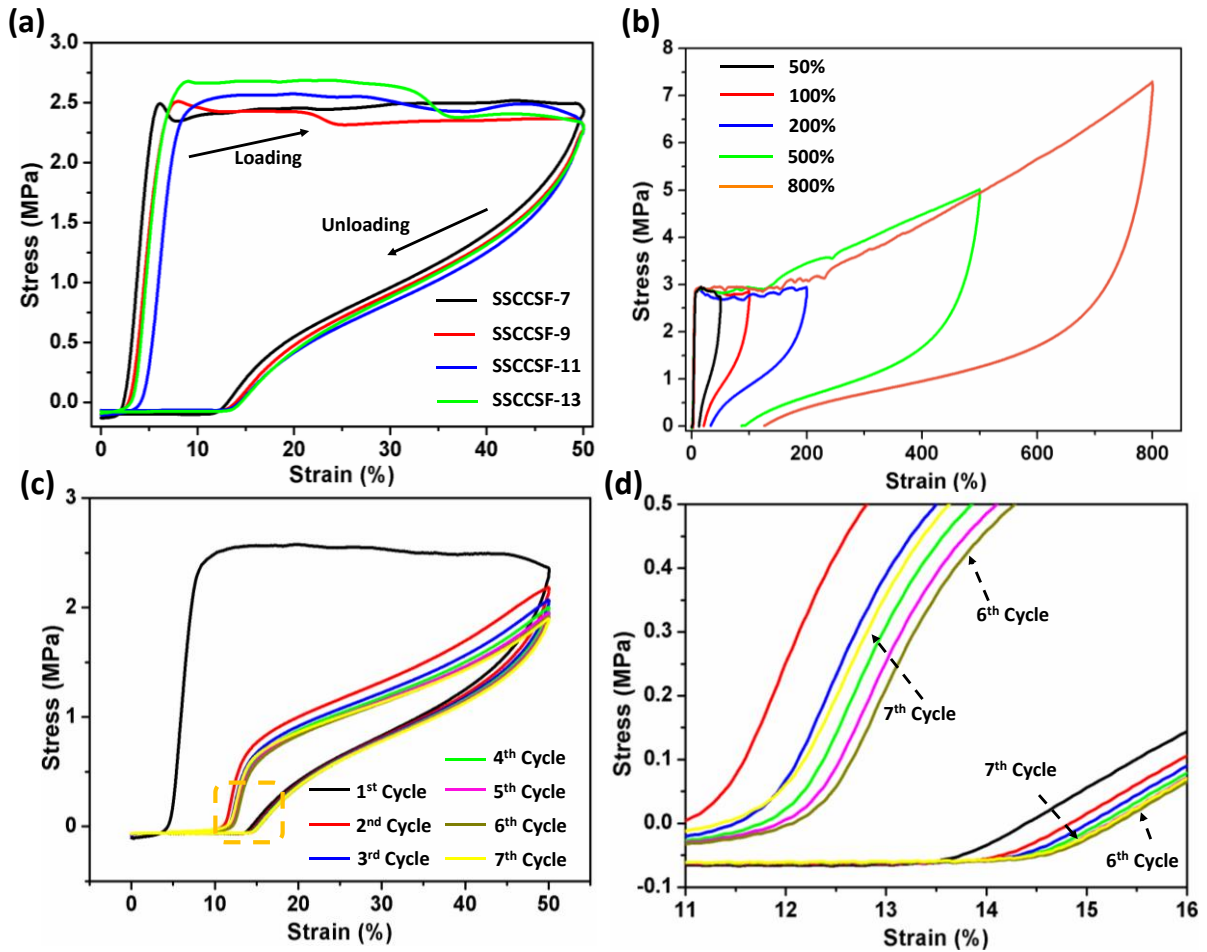
Figure 4. (a) Elastic recovery curves of SSCCSFs with strain of 50%; (b) Elastic recovery curves of SSCCSF-11 under 50%, 100%, 200%, 500% and 800% strain; (c) Seven elastic recovery cycles of SSCCSF-11 under 50% with magnification (d) (The first 6 cycles were continuous and the 7th cycle was 30 s later after the 6th cycle was finished).
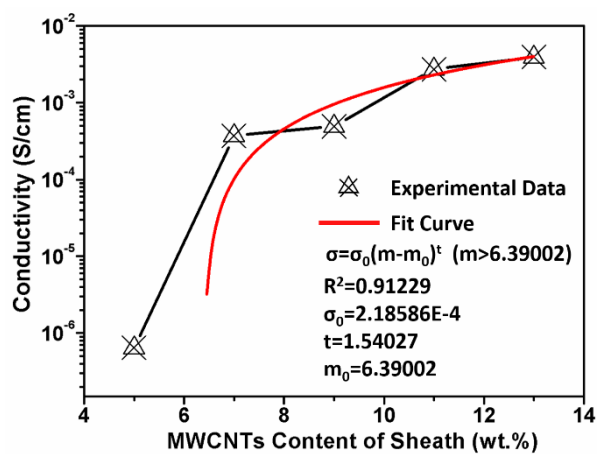
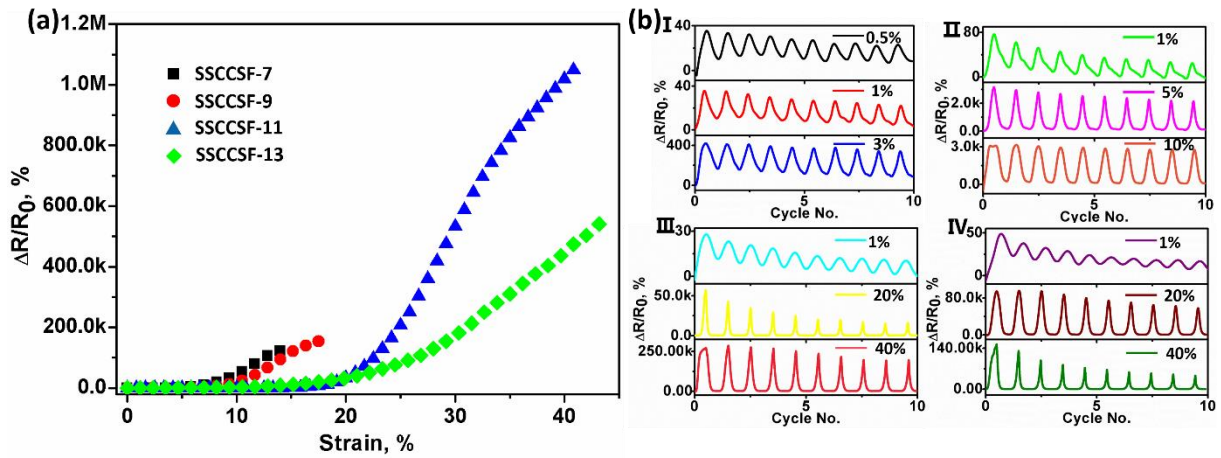**Figure 5. The electrical properties of SSCCSFs**

Figure 6. (a) The *ΔR/R₀*-strain curves of SSCCSFs with different MWCNTs content; (b) The *ΔR/R₀*-Cycle No. curves of SSCCSFs for different strain at a rate of 10 mm/min with I for SSCCSF-7, II for SSCCSF-9, III for SSCCSF-11 and IV for SSCCSF-13.
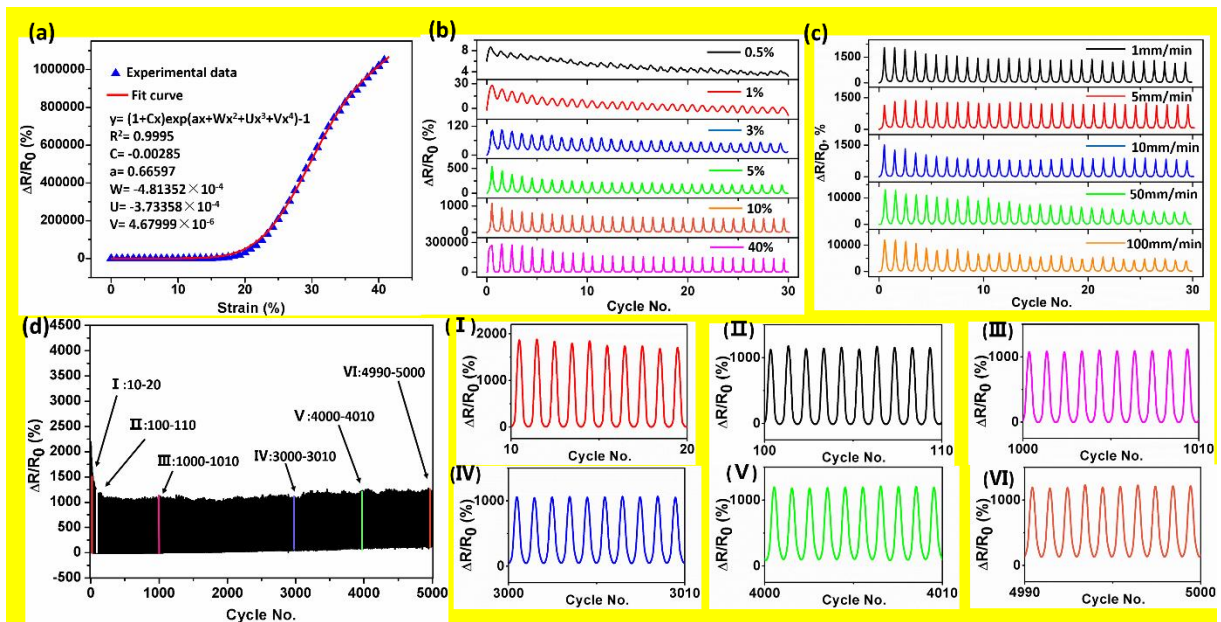

Figure 7. (a) The *ΔR/R₀*-strain fitting curve of SSCCSF-11; (b) The relative resistance change with repeated cycles at different strains for SSCCSF-11 at a fixed rate of 5 mm·min⁻¹; (c) The relative resistance variation with repeated cycles at different strain rates for the SSCCSF-11 (the strain was fixed at 10%); (d) The relative resistance variation for 5000 cycles at 0-10% strain at 10 mm·min⁻¹.
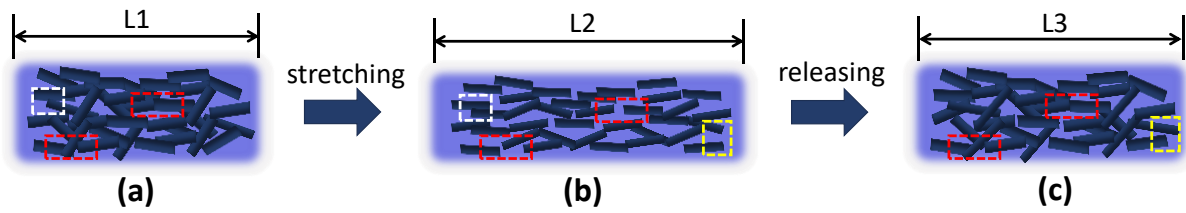
Figure 8. A schematic illustration of the stretching-releasing process mechanism
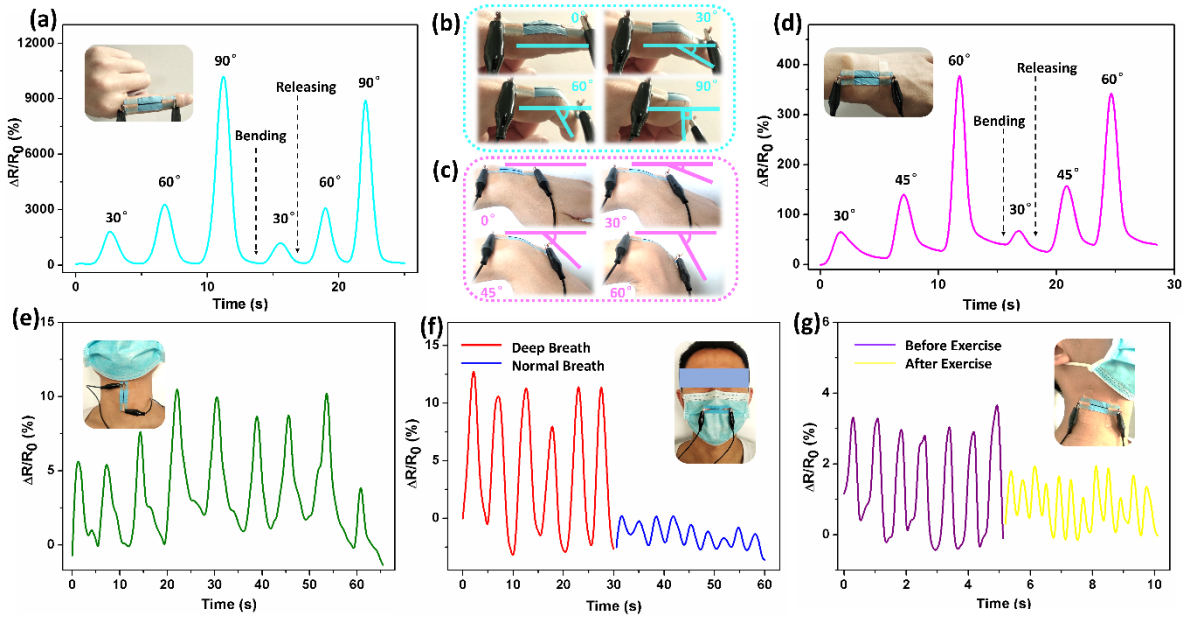

Figure 9. Application of SSCCSF strain sensor in monitoring human motion with the length of 2 cm. (a) The interphalangeal joint bending test under different angles of 30 °,60 °, 90 ° with diagrams (b); (d) The wrist joint bending test under different angles of 30 °,45 °,60 ° with diagrams (c); (e) Swallowing behavior test; (f) Breathing test, (g) The carotid artery test.

Table of Contents

A poly (styrene-butadiene-styrene) (SBS)/multi-walled carbon nanotubes (MWCNTs) core-sheath fiber (SSCCSF) strain sensor was fabricated via coaxial wet-spinning method, which has high sensitivity in broad working range (Gauge Factor = 25832.77 at 41.5% strain) and

excellent durability (5000 cycles). The strain sensor can detect human motions including hand

joint bending (such as knuckles and wrists), swallowing, breathing and pulse beat.